SIMULATION OF VOLTAGE DIP EVENT IN FIXED-SPEED WIND TURBINES: FATIGUE EVALUATION

Badrinath Veluri*, David Santos-Martin**, Henrik Myhre Jensen*

Grid code modifications require the in service fixed speed wind turbines to ride-trough grid faults. Voltage dips due to electrical grid faults generate transients of the generator electromagnetic torque. These transients result in significant stresses and vibrations affecting the fatigue life of the components. An electro-mechanical model was built to simulate the grid faults that excite the asynchronous generator with poorly damped stator flux oscillations. These oscillations cause transients of the generator electromagnetic torque. This article focuses in estimating the resulting significant stresses transients affecting the fatigue life of drivetrain system due to voltage dips. A rainflow cycle counting method was developed to evaluate the fatigue life of the mechanical system. The methodology analyses the stress history and estimates the mean and amplitudes of the counted cycles, and time of duration to calculate the accumulated damage occurred during the voltage dip event.

Keywords: *voltage dip, electro-mechanical model, drivetrain, induction generator, rainflow count, fatigue*

1. Introduction

Increased environmental consciousness has driven the increased capacity of wind power over the years. Grid connected Wind Turbines (WT) experiences network disturbances of various kinds, thus generating control problems of frequency and voltage in the system. Network disturbances leading to voltage dips develop the transients in the electromagnetic torque of the generator. These transients propagate through the upstream of the transmission system stressing the drivetrain components [1–4]. Severe operating Drivetrain failures in WT's have characterized the past of this industry and have prevented turbines in achieving their intended 20-year design life. Available certification standards like IEC 61400-1 [5] details a list with different design situations and load cases, that the wind turbines have to be designed to withstand these disturbances, without stating the requirements in terms of specific faults that are detailed in grid codes. In the recent years some authors have studied the voltage dip effects both from an electrical perspective and with mechanical interest focusing on the temporal transient loads of blades, tower and the drivetrain system [6–8].

The fixed speed wind turbine couples the dynamics of the wind directly to the grid through the induction generator, which causes a poor quality power output of the turbine. The current study presents a novel approach in simulating the voltage dip impact for a typical grid connected wind turbines. The severity of such disturbances on the fatigue life of drivetrain components was analysed by rainflow analysis developed in the framework of [9]

* Mr. B. Veluri, Dr. techn. H. M. Jensen, Aarhus School of Engineering, Aarhus University, Dalgas Avenue 4, 8000 Aarhus C, Denmark

** D. Santos-Martin, Department of Electrical Engineering, University Carlos III, Madrid, Spain

for fatigue evaluation. A computational model was built in MATLAB/Simulink environment containing detailed sub system considering the interaction aspects. This article deals with the modeling and implementation of different components of the wind turbine in the form of a library, which gives a variety of simulation possibilities. This model provides a better understanding of the mechanical behavior and fatigue implications in drivetrain components of the wind turbine system involving a main limitation of available technical data.

2. Wind turbine model description

A brief description of electro-mechanical model that describes the electrical and mechanical components of the Fixed Speed Wind Turbine (FSWT) connected to the grid as shown in Figure. 1.

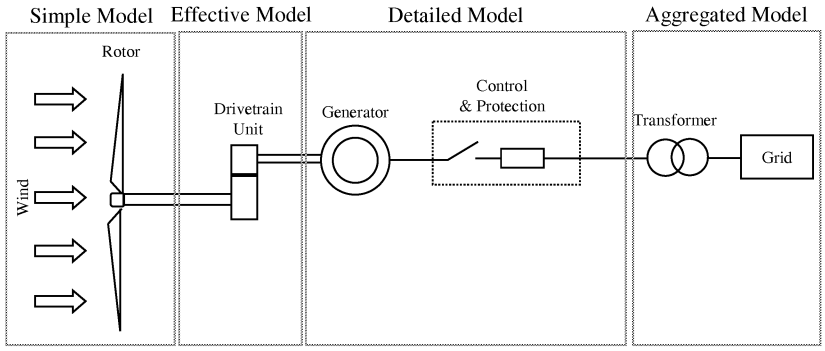

Fig.1: Schematic modeling of the Fixed Speed Wind Turbine

2.1. Aerodynamic model

The aerodynamic torque T_{aero} on the drivetrain of a wind turbine varies continuously over the time due to the proper unsteady and non-linear characteristics of the complex aerodynamics was defined by

$$T_{\text{aero}} = C_{\text{p}}(\lambda, \beta)\, P_{\text{v}} = \frac{1}{2\,\omega_{\text{rot}}}\, \varrho_{\text{air}}\, v^3 A\, C_{\text{p}}(\lambda, \beta)\ . \tag{1}$$

The relation between C_{p} performance coefficient and λ tip speed ratio is normally established by the using the generic equation as stated in [10] for different values of β blade pitch angle. Where v is the wind velocity, A is the frontal area swept by the rotor, ω_{rot} angular speed of the rotor respectively.

2.2. Drivetrain model

The aerodynamic torque variations due to wind turbulence are directly transferred to the dynamic mechanical transmission system. The electrical generator runs in a relatively high speed compared to the aerodynamic rotor. In the drivetrain a low speed shaft (LSS) in the rotor side are connected to a high speed shaft (HSS) in the electrical generator side by using a gearbox. A detailed investigation with a reduced number of DOF is adopted for analyzing dynamic behavior [11, 12]. Any restrictions on movement (linkages) between the bodies are realized with joints with specific properties. Such mechanical systems are described mathematically by coupled ordinary differential and algebraic equations.

These variations are directly transferred to the dynamic mechanical transmission system. A reduced 2-DOF model with simple inertia representation of the drivetrain containing the gear box is shown in Figure 2. In this model the next considerations were made : rotor, gears and LSS are rigid bodies and HSS is flexible. The equations of motion can be expressed

$$J_{\mathrm{rot}} \frac{\mathrm{d}\omega_{\mathrm{rot}}}{\mathrm{d}t} = T_{\mathrm{aero}} - T_{\mathrm{rot}} \ , \tag{2}$$

$$J_{\mathrm{mech}} \frac{\mathrm{d}\omega_{\mathrm{mech}}}{\mathrm{d}t} = T_{\mathrm{mech}} - K\,(q_2 - q_3) - D\,(\omega_{\mathrm{mech}} - \omega_{\mathrm{gen}}) - T_{\mathrm{gen}} \ , \tag{3}$$

$$J_{\mathrm{gen}} \frac{\mathrm{d}\omega_{\mathrm{gen}}}{\mathrm{d}t} = T_{\mathrm{gen}} - T_{\mathrm{elec}} \ , \tag{4}$$

where T_{mech} is the mechanical torque available at the high speed shaft connected to the generator, T_{gen} is the mechanical torque available at the shaft of the induction generator, T_{elec} is the electromagnetic torque in the induction generator, K is the equivalent stiffness of the shaft with D as the equivalent damping coefficient.

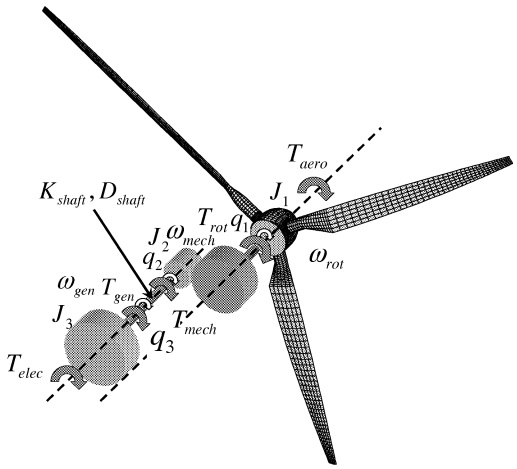

Fig.2: Dynamic representation of WT drivetrain

2.3. Induction Generator model

Applying the standard modeling assumptions of linearity to the magnetic circuits and sinusoidal distributed stator windings, the general complex vector model of an induction machine (IM) in the synchronous reference frame as shown in Figure 3 [13] can be expressed as

$$\begin{aligned} \bar{u}_{\mathrm{s}} &= R_{\mathrm{s}}\,\bar{i}_{\mathrm{s}} + \frac{\mathrm{d}\bar{\phi}_{\mathrm{s}}}{\mathrm{d}t} + \mathrm{j}\,\omega_{\mathrm{s}}\,\bar{\phi}_{\mathrm{s}} \ , \\ 0 &= R_{\mathrm{r}}\,\bar{i}_{\mathrm{r}} + \frac{\mathrm{d}\bar{\phi}_{\mathrm{r}}}{\mathrm{d}t} + \mathrm{j}\,s\,\omega_{\mathrm{s}}\,\bar{\phi}_{\mathrm{r}} \ , \\ \bar{\phi}_{\mathrm{s}} &= L_{\mathrm{s}}\,\bar{i}_{\mathrm{s}} + L_{\mathrm{m}}\,\bar{i}_{\mathrm{r}} \ , \\ \bar{\phi}_{\mathrm{r}} &= L_{\mathrm{m}}\,\bar{i}_{\mathrm{s}} + L_{\mathrm{r}}\,\bar{i}_{\mathrm{r}} \ , \end{aligned} \tag{5}$$

where u_{s} is the stator voltage; i_{s} and i_{r} are the stator and rotor currents; ϕ_{s} and ϕ_{r} are the stator and rotor flux linkages; L_{s}, L_{r} are the stator and rotor inductance; L_{ds}, L_{dr} are the

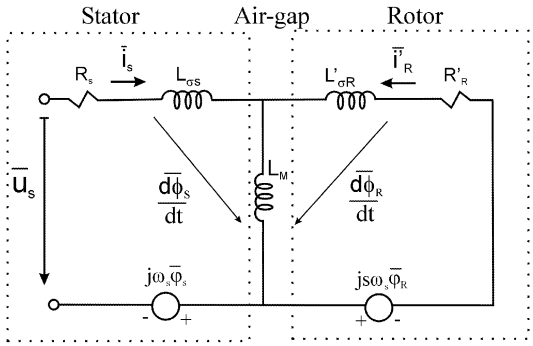

Fig.3: Induction Machine equivalent circuit of dynamic model in asynchronous reference frame

stator and rotor leakage inductance; R_s, R_r are the stator and rotor resistances respectively; ω_s is the grid pulsation and s the slip parameter.

Matrix formulation of the considered model was given by

$$\begin{gathered}\frac{\mathrm{d}}{\mathrm{d}t}\begin{bmatrix}\bar{\phi}_\mathrm{s}\\ \bar{\phi}_\mathrm{r}\end{bmatrix} = -\begin{bmatrix}R_\mathrm{s} & 0\\ 0 & R_\mathrm{r}\end{bmatrix}\begin{bmatrix}\bar{i}_\mathrm{s}\\ \bar{i}_\mathrm{r}\end{bmatrix} - \mathrm{j}\,\omega_\mathrm{s}\begin{bmatrix}1 & 0\\ 0 & s\end{bmatrix}\begin{bmatrix}\bar{\phi}_\mathrm{s}\\ \bar{\phi}_\mathrm{r}\end{bmatrix} + \begin{bmatrix}\bar{u}_\mathrm{s}\\ 0\end{bmatrix}\ ,\\ \begin{bmatrix}\bar{i}_\mathrm{s}\\ \bar{i}_\mathrm{r}\end{bmatrix} = \begin{bmatrix}L_\mathrm{s} & L_\mathrm{m}\\ L_\mathrm{m} & L_\mathrm{r}\end{bmatrix}^{-1}\begin{bmatrix}\bar{\phi}_\mathrm{s}\\ \bar{\phi}_\mathrm{r}\end{bmatrix}\ .\end{gathered} \tag{6}$$

These algebraic-differential equations (6) can be expressed as a state variable model of fluxes (7) with $\mathbf{U}$ as an exogenous or perturbation variable

$$\frac{\mathrm{d}}{\mathrm{d}t}\mathbf{\Psi} = \mathbf{A}_\phi(t)\,\mathbf{\Psi} + \mathbf{U}\ . \tag{7}$$

The homogeneous time varying linear system associated to (7) in homogeneous form is

$$\frac{\mathrm{d}}{\mathrm{d}t}\mathbf{\Psi} = \mathbf{A}_\phi(t)\,\mathbf{\Psi}\ . \tag{8}$$

The time-variant and complex coefficients matrix $\mathbf{A}_\phi$ can be approximated by

$$\mathbf{A}_\phi = \begin{bmatrix}-\dfrac{R_\mathrm{s}\,L_\mathrm{r}}{\sigma L_\mathrm{s}\,L_\mathrm{r}} - \mathrm{j}\,\omega_\mathrm{s} & \dfrac{R_\mathrm{s}\,L_\mathrm{m}}{\sigma L_\mathrm{s}\,L_\mathrm{r}}\\ \dfrac{R_\mathrm{r}\,L_\mathrm{m}}{\sigma L_\mathrm{s}\,L_\mathrm{r}} & -\dfrac{R_\mathrm{r}\,L_\mathrm{s}}{\sigma L_\mathrm{s}\,L_\mathrm{r}} - \mathrm{j}\,s\,\omega_\mathrm{s}\end{bmatrix} \approx \begin{bmatrix}-\dfrac{R}{2\,L_\mathrm{d}} - \mathrm{j}\,\omega_\mathrm{s} & \dfrac{R}{2\,L_\mathrm{d}}\\ \dfrac{R}{2\,L_\mathrm{d}} & -\dfrac{R}{2\,L_\mathrm{d}} - \mathrm{j}\,s\,\omega_\mathrm{s}\end{bmatrix}\ , \tag{9}$$

where L_d and R are the average value of stator and rotor leakage inductances and resistance respectively. The asynchronous generator dynamics can be characterized by the time-varying linear model (8) in the homogeneous form or by (7) when considering disturbances.

This model can be linearized at the equilibrium point ψ_0, and being considered, locally, as a time-invariant system

$$\frac{\mathrm{d}}{\mathrm{d}t}\mathbf{\Psi} = (\mathbf{A}_\phi)_{\Psi 0}\,\mathbf{\Psi} = \mathbf{A}_{\phi 0}\,\mathbf{\Psi}\ . \tag{10}$$

The solution to (10) can be developed in terms of the known state-transmission matrix that in this case takes the form of the matrix exponential function in the time domain and when

using the Laplace transform yields in

$$\boldsymbol{\Psi}(t) = \mathrm{e}^{\mathbf{A}_{\phi 0}\, t}\, \boldsymbol{\Psi}(0)\ , \tag{11}$$

$$\boldsymbol{\Psi}(s) = (s\,\mathbf{I} - \mathbf{A}_{\phi 0})^{-1}\, \boldsymbol{\Psi}(0) = \frac{\mathrm{adj}(s\,\mathbf{I} - \mathbf{A}_{\phi 0})}{|s\,\mathbf{I} - \mathbf{A}_{\phi 0}|}\, \boldsymbol{\Psi}(0)\ . \tag{12}$$

The roots of the characteristic $|s\,\mathbf{I} - \mathbf{A}_{\phi 0}|$ equation, called also Eigenvalues of the homogeneous system or poles of the transfer function within the frequency-domain, characterizes locally the dynamic behavior of (10). From equations (10), (11) and (12) the roots $|\lambda\,\mathbf{I} - \mathbf{A}_{\phi 0}|$ of it can calculated and verified with reference to the Figure 3 that the Eigenvalues of the system can be approximated by the diagonal terms of the matrix

$$\lambda_1 \approx -\frac{R}{2\,L_\mathrm{d}} - \mathrm{j}\,\omega_\mathrm{s}\ , \tag{13}$$

$$\lambda_2 \approx -\frac{R}{2\,L_\mathrm{d}} - \mathrm{j}\,s\,\omega_\mathrm{s}\ . \tag{14}$$

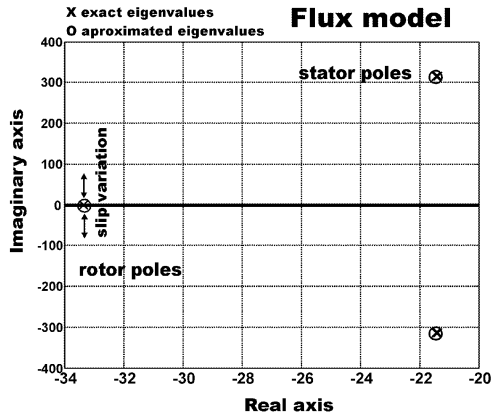

Fig.4: Example of poles location of the linearized induction machine model while changing the slip parameter

The electromagnetic torque T_elec of the generator is a scalar value which dynamics depend only on the stator and rotor flux (8), being shown in equations (13) and (14) and Figure 4 that the former are poorly damped when a perturbation occurs

$$T_\mathrm{elec} = \frac{3}{2}\,P_\mathrm{p}\,\frac{L_\mathrm{m}}{\sigma\,L_\mathrm{s}\,L_\mathrm{r}}\,|\bar{\phi}_\mathrm{r} \wedge \bar{\phi}_\mathrm{s}| = \frac{3}{2}\,P_\mathrm{p}\,\frac{L_\mathrm{m}}{\sigma\,L_\mathrm{s}\,L_\mathrm{r}}\,\mathrm{Im}(\bar{\phi}_\mathrm{r}^{*}\,\bar{\phi}_\mathrm{s})\ , \tag{15}$$

where P_p the number of the generator pole is pairs; Im is the imaginary part of the scalar product of the two vectors and leakage coefficient is $\sigma = 1 - L_\mathrm{m}^2/(L_\mathrm{s}\,L_\mathrm{r})$.

2.4. Network model

The complete electrical diagram including the network is shown in Figure 5. The main components are the generator, wind turbine transformer (T1), feeder line and the grid. The

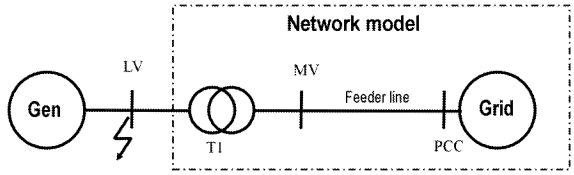

Fig.5: Single circuit diagram of FSWT connected to electric grid

former has been detailed previously; the feeder line and the transformer parameters are resumed in the Appendix.

Some grid standards [14] recommend modeling this grid with a dynamic model containing the following nodes : a node UCTE with a static synchronous generator that represents the system inertia and a load demand; a node with a dynamic synchronous generator model and a load demand; and finally the typical line model. Another option is use a Thevenin equivalent. Next it is explained how the wanted characteristics of the voltage dip define the grid model.

Voltage dips are short duration reductions in root mean square of voltage magnitude, caused by short circuits, overloads and starting of large motors. These faults may cause the trip of wind turbines. The main causes of severe voltage dips are short circuits and earth faults in the grid. The fault current causes a drop over a wide part of the network, and the voltage starts to recover when the protection clears the fault or the fault disappear itself. Different types of faults lead to different type of dips [15]. So far there is no consensus on the grid requirements and each Transmission System Operator (TSO) is publishing their grid codes [16] with the values and types of dips that wind turbines must support without tripping.

When a fault is applied to the wind turbine terminals the voltage for each phase has a characteristic signature [17]. In a simulation this can be replicated with the complex dynamic model of the grid. An approximate result may be obtained with a static grid: linear impedance and stiff grid (Thevenin equivalent). The total impedance module and its angle will characterize the profile of the voltage [18].

Each grid code defines a typical voltage tolerance curve as the maximum required to the WT to support. The so-called voltage tolerance curve is a useful tool to describe immunity of equipment against voltage dips at its terminals. When testing existing equipment against tolerance requirements, it is not necessary to obtain the complete curve, but during the design and development stage the voltage tolerance curve is a good tool to describe the performance [19]. The voltage tolerance curve, and therefore the grid and fault [14] parameters that are listed in the appendix, chosen for this study corresponds to a square curve with varying depths of 0.7 p.u., 0.85 p.u, and 0.9 p.u. for a duration of 500 ms. This fault will excite harder all the electrical and mechanical modes than a softer curve, so the approach is considered conservative.

3. Rainflow counting and fatigue model

Fatigue is a major concern during the various stages of design, manufacturing and operation. To have better understand of the fatigue behavior of the system vitual testing procedures adds a considerable value to the design process or in-service components thus reducing the evaluation time that is required for fatigue test. In the present context fatigue

model was developed in the framework of linear Palmgren-Miner hypothesis. In the event of voltage dip the fatigue load cycles thus increasing the fatigue damage in a cummulative manner and remains an unresolved situation.

3.1. Rainflow counting model

In the present article a methodolgy has been developed to estimate the rainflow count in the framework [9] for the stress history developed during the voltage dip event thus estimating the mean stresses and the amplititude of the stress and the respective duration which is used to estimate the cummulative damage incurred for each such voltage dip event during the service of the wind trubine system. The developed model in the SIMULINK environment estimates the torque transients at various stages of the wind trubine system during the specified voltage dip event as a function of respective time duration. In the present study we restricted to concentrate only on the low speed shaft stress history estimated from the torque transients developed during the voltage dip event.

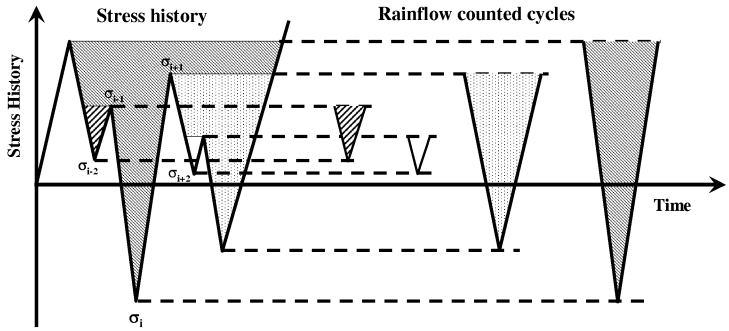

Fig.6: Stress history and the corresponding rainflow counted cycles

Rainflow count is identified as shown in Figure 6 between any two adjacent reversals in the stress history by satisfying the following

$$|\sigma_{i-1} - \sigma_i| < |\sigma_i - \sigma_{i+1}| \ . \tag{16}$$

The stress amplitude $\sigma_{\mathrm{a}i}$ for each counted cycle is estimated as follows

$$\sigma_{\mathrm{a}i} = \frac{|\sigma_{i-1} - \sigma_i|}{2} \ . \tag{17}$$

The mean stress $\sigma_{\mathrm{m}i}$ for such cycles are estimated from the following

$$\sigma_{\mathrm{m}i} = \frac{\sigma_{i-1} + \sigma_i}{2} \ . \tag{18}$$

3.2. Fatigue model

On the assumption of the linear Palmgren-Miner hypothesis of damage accumulation and the stress-life fatigue characteristics of the material, the damage-time function was determined. The load segments, where the influence on the material fatigue was significant, were determined on the basis of the fixed damage-intensity level.

The mean and the amplitudes of the stress history ($\sigma_{\mathrm{a}i}$ and $\sigma_{\mathrm{m}i}$) are estimated in order to calculate the damage D_i caused by the torque transients during the voltage event by the following

$$D_i = \frac{n_i}{N_{\mathrm{f}i}(\sigma_{\mathrm{a}i}, \sigma_{\mathrm{m}i})} \ , \tag{19}$$

where n_i is equal to 1 for a cycle and 0.5 for a half cycle, $N_{\mathrm{f}i}(\sigma_{\mathrm{a}i}, \sigma_{\mathrm{m}i})$ is the function returning a number of cycles to failure according to the amplitude $\sigma_{\mathrm{a}i}$ and the mean value $\sigma_{\mathrm{m}i}$ determined from the stress cycle and the fatigue characteristics of the material that are estimated by Marrow stress-life characteristics.

$$\sigma_{\mathrm{a}} = (\sigma'_{\mathrm{f}} - \sigma_{\mathrm{m}})(2\,N_{\mathrm{f}})^b \ , \tag{20}$$

$$N_{\mathrm{f}i} = \frac{1}{2}\left(\frac{\sigma_{\mathrm{a}i}}{\sigma'_{\mathrm{f}} - \sigma_{\mathrm{m}i}}\right)^{1/b} \ , \tag{21}$$

where σ'_{f} the fatigue strength coefficient and b is the fatigue strength exponent. In the present investigations $\sigma'_{\mathrm{f}} = 1000\,\mathrm{MPa}$ and $b = -0.15$ [20] are considered for estimating the damage accumulated during the voltage dip event.

Computation of the fatigue damage caused by the considered loading interval T_0 duration of voltage dip is usually realized with the assumption of hypothesis of the linear fatigue damage accumulation. The proven Palmgren-Miner hypothesis assumes that the total damage occurred per voltage dip event can be expressed as the sum of particular damages caused by distinguished cycles is given by

$$D = \sum_{i=1}^{k} D_i \ , \tag{22}$$

where k is the number of cycles that are calculated from the random loading history.

4. Results and Discussion

To study the impact of mechanical stress transients during the voltage the simulations were carried out at a wind speed of $10\,\mathrm{m\,s^{-1}}$. The speed was choosen considering that more mechanical vibration occurs during operation of wind turbine at stall condition. The simulation parameters tabulated in Table 1 and Table 2, for 500 ms of fault duration with voltage dip severities of 70 %, 85 % and 90 %, as mentioned in [21] with constant wind speed. Figure 7 depicts the voltage dip event for various severities and their respective torque transients in the electromagnetic torque variation at the generator end and it transformation to the upstream drivetrain system is observed through the torque variations on low speed side. The troque transients are normalized with the specified operating torque rating as per operating guidelines framework in IEC 61400-1 [5]. It is very important to notice that the quantitative results of this case study for various voltage dip severieties are not necessarily representative for other wind turbines of the same type, since they depend critically on the drivetrain torsional characteristics, as well as on the generator parameters.

These torsional variations in the drivetrain system during the short term will affect the overall performance of the system. These implications of torque transients are used to estimate the stress levels in the vaious stages of the drivetrain system for the evaluation of fatigue implication on the WT drivetrain system. The corresponding normalized stress

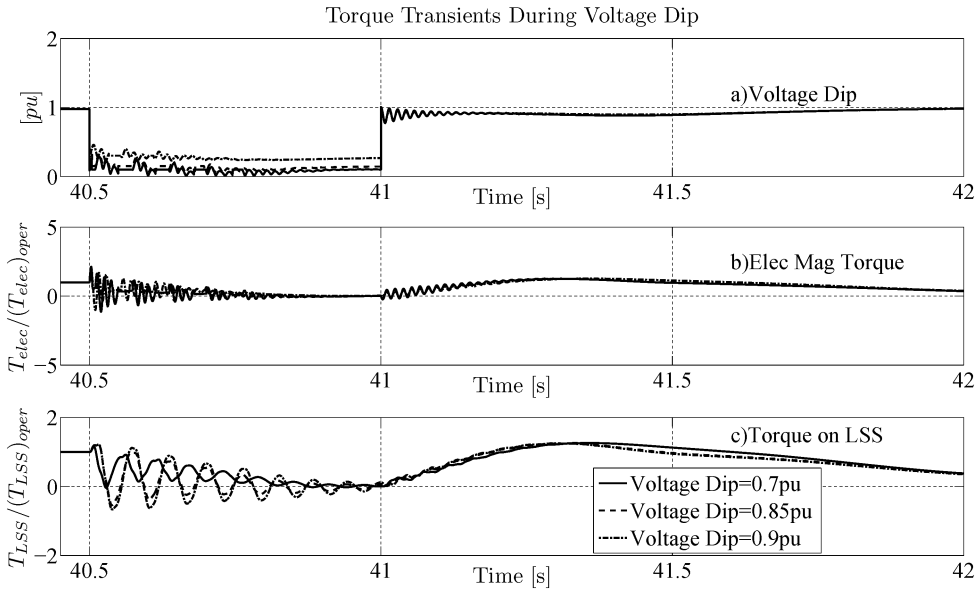

Fig.7: Normalized torque transients for wind speed 10 m/s with varying severity (a) Voltage Dip event, (b) Electromagnetic torque, (c) Torque on Low-speed shaft

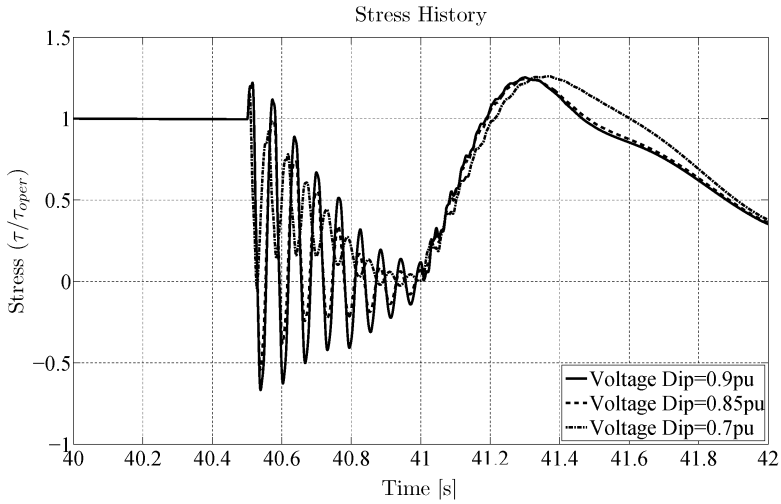

Fig.8: Normalized stress History during the Voltage Dip event for varying severities

history at the low speed shaft side (LSS) was estuimated during the voltage dip event is estimated and is depicted in Figure 8.

In order to quantify the impact of voltage dip on the drivetrain system, using the rainflow analysis the mean and amplitude of the stress transients which are developed during the voltage dip event are estimated. Figures 9, 10 and 11 depicts the mean and amplitude of stress transients on low speed shaft with varying voltage dip severities. The severieties are considering inorder to simulate the design load cases specified in IEC 61400-1 [5].

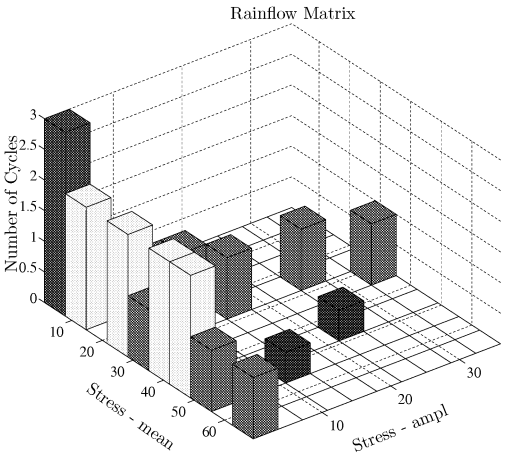

Fig.9: Estimated rainflow matrix of the stresses registered on LSS 0.7 p.u. voltage dip severity

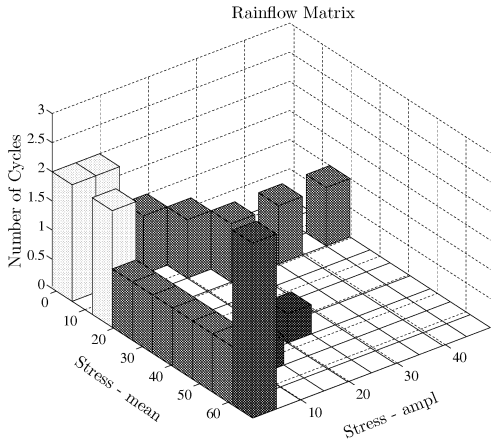

Fig.10: Estimated rainflow matrix of the stresses registered on LSS 0.85 p.u. voltage dip severity

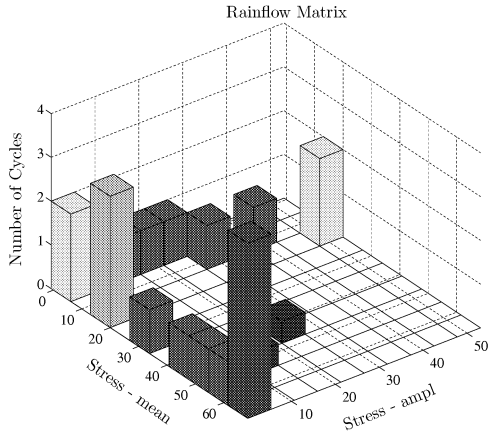

Fig.11: Estimated rainflow matrix of the stresses registered on LSS 0.9 p.u. voltage dip severity

Upon estimating the mean and amplititude of the random stress history and their respective duration for the stated voltage dip servieties, from equations (19) and (21). The fatigue damage caused by counted cycle is presented in Figure 12 for a voltage dip severity of 0.9 p.u. for duration of 500 ms. Depending upon the stress intensities the accumulated damage is estimated some of the stress cycles do not cause damage which is eveident from the Figure 12.

5. Summary

The focus of this article is mainly on analyzing the impact of stress transients developed in the drivetrain system during the voltage dip event. The attention is also drawn to how to access a throughout insight on the grid faults impact on the wind turbine structural loads and to investigate the whole integrated wind turbine design with focus simultaneously on both structural and electrical design aspects. In this respect, a simulation approach for the

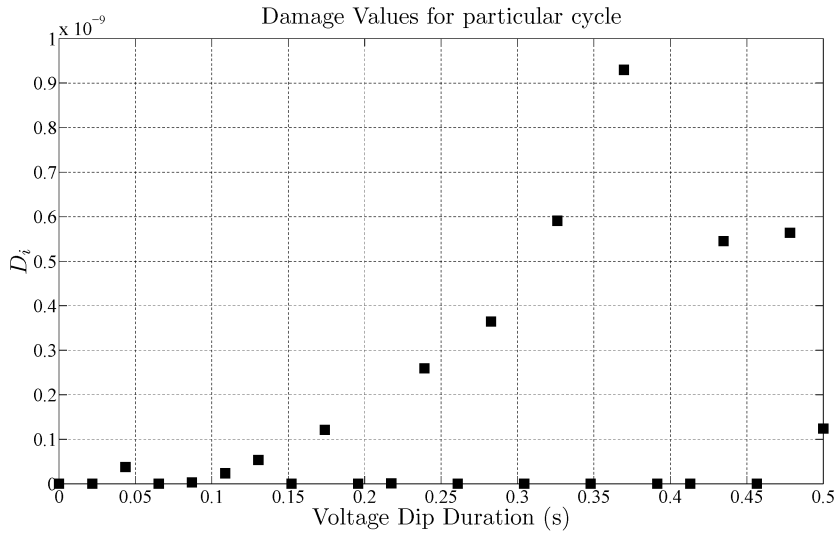

Fig.12: Damage values for particular cycles for 0.9 p.u. voltage dip severity

quantification of torque transients, caused by the network disturbances has been proposed and exemplified for a case study of an active stall wind turbine and a 500 ms three phase short circuit fault on the grid. In order to quantify how the grid faults and grid codes fulfillment do affect the wind turbine loads and thus its lifetime, a rainflow analysis of the stress transients on the low speed side of the drivetrain system has been performed and compared for three cases of voltage dip severities for a constant wind speed. Rainflow analyses for fatigue and ultimate loads in the drivetrain system, respectively, have been accomplished.

Appendix

Parameter	Value	Units
Number of blades	3	–
Rated wind/Simulation speed	15/10	$\mathrm{m\,s^{-1}}$
Rotor inertia	115	$\mathrm{kg\,m^2}$
Drivetrain torsional damper	10^7	$\mathrm{N\,m\,s^{-1}}$
Drivetrain torsional spring	10^9	$\mathrm{N\,m\,rad^{-1}}$
Gearbox ratio	80	–
Gearbox inertia	80	$\mathrm{kg\,m^2}$
Generator inertia	50	$\mathrm{kg\,m^2}$

Tab.1: FSWT characteristics parameters

Parameter	Symbol	Value	Units
Base power	S_n	1.65	MVA
Base voltage	V_n	0.69	kV
Slip at base power	s	0.017	p.u.
Stator resistance	R_s	0.0048	p.u.
Rotor resistance	R_r	0.0044	p.u.
Stator leakage inductance	L_s	0.1248	p.u.
Rotor leakage inductance	L_r	0.1791	p.u.
Mutual inductance	L_m	6.77	p.u.

Tab.2: Induction generator parameters

References

[1] Bollen M.H.J., de Graaff R.A.A.: Behavior of AC and DC drives during voltage sags with phase-angle jump and three-phase unbalance, Power Engineering Society, Winter Meeting, IEEE 1999; 2:1225–1230, vol. 2

[2] IEEE Recommended Practice for the Design of Reliable Industrial and Commercial Power Systems, IEEE STD 493-2007 (Revision of IEEE Std 493-1997) 2007:1–383

[3] Brekken T., Mohan N., Undeland T.: Control of a doubly-fed induction wind generator under unbalanced grid voltage conditions, Power Electronics and Applications, 2005 European Conference on 2005:10 pp., p. 10

[4] Garcia J.M., Domínguez-Navarro J.A.: Behaviour improvement during faults of fixed speed stall control induction generator wind turbines, Wind Energy 2009, 12:527–41
[5] IEC 61400-1. Wind turbine Part 1: Design requirements Edition 3, IEC report 88/228/FDIS, International Electrotechnical Commission, 2005
[6] Hansen A.D., Cutululis N.A., Markou H., Sørensen P.E.: Impact of fault ride-through requirements on fixed-speed wind turbine structural loads, Wind Energy 2010
[7] Papathanassiou S.A., Papadopoulos M.P.: Mechanical stresses in fixed-speed wind turbines due to network disturbances. Energy Conversion, IEEE Transactions on 2001, 16:361–7
[8] Fadaeinedjad R., Moschopoulos G., Moallem M.: Investigation of voltage sag impact on wind turbine tower vibrations, Wind Energy 2008, 11:351–75
[9] ASTM E-1049-85 (2005). Standard Practices for Cycle Counting in Fatigue Analysis, ASTM International, West Conshohocken, PA, 10.1520/C0033-03E01, www.astm.org
[10] Anderson P.M., Bose A.: Stability Simulation of Wind Turbine Systems, Power Apparatus and Systems, IEEE Transactions on 1983, PAS-102:3791–5
[11] Baruh H.: Analytical Dynamics, McGraw Hill, 1999
[12] Ramtharan G., Jenkins N., Anaya-Lara O., Bossanyi E.: Influence of rotor structural dynamics representations on the electrical transient performance of FSIG and DFIG wind turbines, Wind Energy 2007, 10:293–301
[13] Novotny D.W., Lipo T.A.: Vector Control and Dynamics of AC Drives, New York USA: Oxford University Press, 1996
[14] Ausin J.C., Gevers D.N., Andresen B.: Fault ride-through capability test unit for wind turbines, Wind Energy 2008, 11:3–12
[15] Bollen M.: Voltage Sags and Interruptions – Understanding Power Quality Problems 1999
[16] Jauch C., Matevosyan J., Ackermann T., Bolik S.: International comparison of requirements for connection of wind turbines to power systems, Wind Energy 2005, 8:295–306
[17] Styvaktakis E., Bollen M.H.J.: Signatures of voltage dips: transformer saturation and multistage dips, Power Delivery, IEEE Transactions on 2003, 18:265–70
[18] Prabha K., Balu Neal J., Lauby Mark G.: Power system stability and control, McGraw-Hill, 1994
[19] Bollen M.H.J., Olguin G., Martins M.: Voltage dips at the terminals of wind power installations, Wind Energy 2005, 8:307–18
[20] Almar-Naess A.: Fatigue Handbook: Offshore Steel Structures, January 1999
[21] Bollen M., McMichael I., Stephens M., Stockman K., Djokic S., Zavoda F.: CIGRE/CIRED/UIE JWG C4.110 – voltage dip immunity of equipment in installations – status April 2008, Harmonics and Quality of Power, 2008 ICHQP 2008 13th International Conference on 2008:1–8

Received in editor's office: July 7, 2011
Approved for publishing: May 15, 2012